IHJPAS. 36(2)2023

Ibn Al-Haitham Journal for Pure and Applied Sciences
Journal homepage: jih.uobaghdad.edu.iq

The Effect of Rotation on the Heat Transfer of a Couple Stress Fluid in A Non-uniform Inclined Asymmetrical Channel with Inclined MHD

Hanaa Abdulhussein
Department of Mathematics,
College of Science, University of Baghdad, Baghdad, Iraq.
hshatty@uowasit.edu.iq

Ahmed M. Abdulhadi
Department of Mathematics,
College of Science, University of Baghdad, Baghdad, Iraq.
ahm6161@yahoo.com

Article history: Received 23 August 2022, Accepted 9 October 2022, Published in April 2023.

doi.org/10.30526/36.2.2987

Abstract

The purpose of this research is to investigate the effects of rotation on heat transfer using inclination magnetohydrodynamics for a couple-stress fluid in a non-uniform canal. When the Reynolds number is low and the wavelength is long, math formulas are used to describe the stream function, as well as the gradient of pressure, temperature, pressure rise and axial velocity per wavelength, which have been calculated analytically. The many parameters in the current model are assigned a definite set of values. It has been noticed that both the pressure rise and the pressure gradient decrease with the rise of the rotation and couple stress, while they increase with an increase in viscosity and Hartmann number. The explanation of parameters is shown graphically by a series of figures using "MATHEMATICA".

Keywords: Non-uniform channel**,** rotation, inclined MHD, Couple stress, Porous medium

1. Introduction

Using a couple stress fluids as a model for describing biologically complicated fluids, such as colloidal fluids, polymeric suspensions, animal and human blood, and lubrication, is extremely beneficial in understanding a wide range of physical issues. One of the numerous models created to describe the reaction explanation of non-Newtonian fluids is the Couple stress fluid model. Non-Newtonian fluids, such as couple stress fluids, are those in which particle size is taken into account and studied by [1-4]. Shit and Ranjit [5] studied the fluid's peristalsis in non-uniform and asymmetric channels when an external magnetic field is provided. Murad and Abdulhadi [6] Analysis of mixed convective heat transfer for peristaltic transport of viscoplastic fluid: perturbation and numerical studies. Abdulla and Hummady [7] considered the influence of sliding speed on channel walls and the effect of nonlinear particle size. To make things even more complicated, non-Newtonian fluids can't be studied with non-slip boundary conditions because it's easy to see how the walls slide. In technology, boundary slip condition fluids can be used to polish artificial hearts. See [8-13] for a list of studies that use this condition.

Researchers have recently looked into how a magnetic field and rotation affect how fluid moves through an asymmetric channel, Abd-Alla and Abo-Dahab [14]. The effects of rotation and MHD on an asymmetric channel through a porous medium where a Jeffrey fluid flows nonlinearly have been looked at by Abdulhadi and Al-Hadad [15]. In porous media with non-symmetric canals, rotating waveform motion in two-dimensional channels of non-Newtonian fluid was explored by Alshareef [16]. For viscoplastic fluid and variable viscosity on peristalsis, they discussed the influence of rotation of the mixture on convection heat transfer analysis by [17, 18].

This study's objective is to examine the effects of rotation on heat transfer with inclination magnetohydrodynamics in a non-uniform channel containing a couple stress fluid. The equation for the governing equation is examined using low Reynolds approximations and long-wavelength assumptions, respectively. Graphs are used to show the impact of various factors on fluid flow.

2. mathematical Formulation

Consider that the effect of a magnetic field and rotation on heat transfer can be explained by a porous medium with an inclined asymmetry of the couple stress fluid.

Let's say $\bar{Y}_* = \widetilde{h_1}\ (\tilde{X}, \tilde{t})$ and $\bar{Y}_* = \widetilde{h_2}\ (\tilde{X}, \tilde{t})$ here is a representation of the channel's top and bottom walls.

$$\widetilde{h_1}\ (\tilde{X}, \tilde{t}) = d_1 + \left(\tilde{X} - c\tilde{t}\right)\tan\tilde{\alpha} + a_1^* \cos\left[\frac{2\pi}{\lambda}(\tilde{X} - c\tilde{t})\right] \tag{1}$$

$$\widetilde{h_2}\ (\tilde{X}, \tilde{t}) = -d_2 - \left(\tilde{X} - c\tilde{t}\right)\tan\tilde{\alpha} - a_2^* \cos\left[\frac{2\pi}{\lambda}(\tilde{X} - c\tilde{t}) + \phi_\circ\right] \tag{2}$$

Where $a_1^* and\ a_2^*$ are the amplitudes of waves λ is wavelength, $\tilde{t}$ is the time c is wave speed , $(0 \leq \phi_\circ \leq \pi)$ the phase difference $\phi_\circ$between the walls of the channel the rectangular Cartesian coordinates are used $\tilde{X}$and $\tilde{Y}$. The channel's axis is measured by $\tilde{X}$, and the transverse axis is measured by $\tilde{Y}$, which is perpendicular to $\tilde{X}$. The constant heights of the upper and lower walls of the channel from the central line are denoted by $d_1 and\ d_2$, respectively. It's worth noting that $\phi_\circ = 0$ corresponds to an asymmetry with out-of-phase waves, whereas $\phi_\circ = \pi$ relates to waves that are in phase. Furthermore, d_1 , d_2, a_2^*, $a_1^*$and $\phi_\circ$ satisfy the condition;

$a_1^{*2} + a_2^{*2} + 2a_1^* a_2^* cos\phi_\circ \leq (d_1 + d_2)^2$.

The governing equations.

$$\frac{\partial \tilde{U}}{\partial \tilde{X}} + \frac{\partial \tilde{V}}{\partial \tilde{Y}} = 0 \tag{3}$$

$$\rho\left(\frac{\partial \tilde{U}}{\partial \tilde{t}} + \tilde{U}\frac{\partial \tilde{U}}{\partial \tilde{X}} + \tilde{V}\frac{\partial \tilde{U}}{\partial \tilde{Y}}\right) - \rho\grave{\Omega}\left(\grave{\Omega}\tilde{U} + 2\frac{\partial \tilde{V}}{\partial \tilde{t}}\right) = -\frac{\partial \tilde{P}}{\partial \tilde{X}} + \mu\nabla^2\tilde{U} - \eta\nabla^4\tilde{U} - \tilde{\sigma}B_*^2 \cos\Phi\left(\tilde{U}\cos\Phi - \tilde{V}\sin\Phi\right) - \frac{\mu}{k_\circ}\tilde{U} + \rho g\dot{\alpha}\,(T - T_\circ)sin\tilde{\alpha} + \rho g sin\tilde{\alpha} \tag{4}$$

$$\rho\left(\frac{\partial \tilde{V}}{\partial \tilde{t}} + \tilde{U}\frac{\partial \tilde{V}}{\partial \tilde{X}} + \tilde{V}\frac{\partial \tilde{V}}{\partial \tilde{Y}}\right) - \rho\grave{\Omega}\left(\grave{\Omega}\tilde{V} - 2\frac{\partial \tilde{U}}{\partial \tilde{t}}\right) = -\frac{\partial \tilde{P}}{\partial \tilde{Y}} + \mu\nabla^2\tilde{V} - \eta\nabla^4\tilde{V} + \tilde{\sigma}B_*^2 \sin\Phi\left(\tilde{U}\cos\Phi - \tilde{V}\sin\Phi\right) - \frac{\mu}{k_\circ}\tilde{V} - \rho g cos\tilde{\alpha} \tag{5}$$

$$\rho C_p\left(\frac{\partial T}{\partial \tilde{t}} + \tilde{U}\frac{\partial T}{\partial \tilde{X}} + \tilde{V}\frac{\partial T}{\partial \tilde{Y}}\right) = \tilde{K}\left(\frac{\partial^2 T}{\partial \tilde{X}^2} + \frac{\partial^2 T}{\partial \tilde{Y}^2}\right) + \mu\left[2\left\{\left(\frac{\partial \tilde{U}}{\partial \tilde{X}}\right)^2 + \left(\frac{\partial \tilde{V}}{\partial \tilde{Y}}\right)^2\right\} + \left(\frac{\partial \tilde{U}}{\partial \tilde{Y}} + \frac{\partial \tilde{V}}{\partial \tilde{X}}\right)^2\right] + \eta\left[\left(\frac{\partial^2 \tilde{U}}{\partial \tilde{X}^2} + \frac{\partial^2 \tilde{U}}{\partial \tilde{Y}^2}\right)^2 + \left(\frac{\partial^2 \tilde{V}}{\partial \tilde{X}^2} + \frac{\partial^2 \tilde{V}}{\partial \tilde{Y}^2}\right)^2\right] + \tilde{\sigma}B_*^2\left(\tilde{U}\cos\Phi - \tilde{V}\sin\Phi\right)^2 \tag{6}$$

Where $\overrightarrow{V'}=(\tilde{U},\ \tilde{V},\ 0)$ be the velocity vector, $\grave{\Omega}$ is rotation, $\dot{\alpha}$ the Coefficient of thermal expansion , $\tilde{P}$ is the fluid pressure , ρ is density of fluid , Φ is the inclination of the magnetic field angle, μ the dynamic viscosity , η is a constant linked to the couple stress, C_p is the specific heat at constant pressure. impact $\overrightarrow{B_*}=(B_* \sin\Phi\ , B_* \cos\Phi\ ,0)$ the magnetic field vector, $k_\circ$ is the permeability parameter ,T is the temperature , g is the acceleration by gravity , $\tilde{\sigma}$ is the fluids electrical conductivity ,$\tilde{K}$ is the thermal conductivity . The induced electric field is not taken into consideration at all, because assuming a low magnetic Reynolds number

The fixed frame's$(\tilde{X}\ ,\tilde{Y})$ flow field and the wave frame's$(\grave{x}\ ,\grave{y})$ wave field are also considered the motions of an unsteady and steady-state . It's important to think about the relationship between the wave $(\grave{x}\ ,\grave{y})$and the fixed frames $(\tilde{X}\ ,\tilde{Y})$ with a velocity of c as they move apart from one another as a result of the transformations below .

$$\grave{v}=\tilde{V}\ ,\ \grave{y}=\tilde{Y}\ ,\mathrm{T}=\tilde{\mathrm{T}}\ ,\ \grave{x}=\tilde{X}-c\tilde{t},\ \ \grave{u}=\tilde{U}-c\ \ ,\ \grave{p}=\tilde{P} \qquad (7)$$

In which $(\grave{u},\grave{v})$ and $(\tilde{U},\tilde{V})$are the waves' and laboratories' velocities, respectively. the governing equations (3) ,(4) ,(5), and (6) be expressed in Wave frame as using the transformations mentioned above.

$$\frac{\partial \grave{u}}{\partial \grave{x}}+\frac{\partial \grave{v}}{\partial \grave{y}}=0 \qquad (8)$$

$$\rho\left((\grave{u}+c)\frac{\partial \grave{u}}{\partial \grave{x}}+\grave{v}\frac{\partial \grave{u}}{\partial \grave{y}}\right)-\rho\grave{\Omega}\left(\grave{\Omega}\,(\grave{u}+c)+2\frac{\partial \grave{v}}{\partial \tilde{t}}\right)$$
$$=-\frac{\partial \grave{p}}{\partial \grave{x}}+\mu\nabla^2\grave{u}-\eta\nabla^4\grave{u}-\tilde{\sigma}B_*^2\cos\Phi\left((\grave{u}+c)\cos\Phi-\grave{v}\sin\Phi\right)-\frac{\mu}{k_\circ}(\grave{u}+c)$$
$$+\rho g\dot{\alpha}\left(\tilde{\mathrm{T}}-\mathrm{T}_\circ\right)\sin\tilde{\alpha}+\ \rho g\sin\tilde{\alpha} \qquad (9)$$

$$\rho\left((\grave{u}+c)\frac{\partial \grave{v}}{\partial \grave{x}}+\grave{v}\frac{\partial \grave{v}}{\partial \grave{y}}\right)-\rho\grave{\Omega}\left(\grave{\Omega}\,\grave{v}-2\frac{\partial \grave{u}}{\partial \tilde{t}}\right)=-\frac{\partial \grave{p}}{\partial \grave{y}}+\mu\nabla^2\grave{v}-\eta\nabla^4\grave{v}+\tilde{\sigma}B_*^2\sin\Phi\,((\grave{u}+c)\cos\Phi-$$
$$\grave{v}\sin\Phi)-\frac{\mu}{k_\circ}\grave{v}\ -$$
$$\rho g\cos\tilde{\alpha} \qquad (10)$$

$$\rho C_p\left((\grave{u}+c)\frac{\partial \tilde{\mathrm{T}}}{\partial \grave{x}}+\grave{v}\frac{\partial \tilde{\mathrm{T}}}{\partial \grave{y}}\right)=\tilde{K}\left(\frac{\partial^2\tilde{\mathrm{T}}}{\partial \grave{x}^2}+\frac{\partial^2\tilde{\mathrm{T}}}{\partial \grave{y}^2}\right)+\mu\left[2\left\{\left(\frac{\partial \grave{u}}{\partial \grave{x}}\right)^2+\left(\frac{\partial \grave{v}}{\partial \grave{y}}\right)^2\right\}+\left(\frac{\partial \grave{u}}{\partial \grave{y}}+\frac{\partial \grave{v}}{\partial \grave{x}}\right)^2\right]+$$
$$\eta\left[\left(\frac{\partial^2\grave{u}}{\partial \grave{x}^2}+\frac{\partial^2\grave{u}}{\partial y^2}\right)^2+\left(\frac{\partial^2\grave{v}}{\partial \grave{x}^2}+\frac{\partial^2\grave{v}}{\partial \grave{y}^2}\right)^2\right]+\tilde{\sigma}B_*^2\left((\grave{u}+c)\cos\Phi-\grave{v}\sin\Phi\right)^2 \qquad (11)$$

To reduce the number of additional parameters, we shall define the following non-dimensional quantities:

$$\left.\begin{array}{l} x=\frac{\grave{x}}{\lambda},\ y=\frac{\grave{y}}{d_1},\ h_1^*(x)=\frac{\widetilde{h_1}\,(\tilde{X})}{d_1},\ \ h_2^*(x)=\frac{\widetilde{h_2}\,(\tilde{X})}{d_1},\theta_\circ=\frac{\tilde{\mathrm{T}}-\mathrm{T}_0}{\mathrm{T}_1-\mathrm{T}_0}\ ,\ u^*=\frac{\grave{u}}{c},\ v^*=\frac{\lambda\grave{v}}{cd_1}\ , \\ t^*=\frac{c\tilde{t}}{\lambda},R_e=\frac{c\rho d_1}{\mu}\ ,\ \delta=\frac{d_1}{\lambda}\ ,\ \mathcal{H}=\mathrm{B}_* d_1\sqrt{\frac{\tilde{\sigma}}{\mu}}\ \ ,\ P_r=\frac{\mu\,C_p}{\tilde{K}}\ ,\gamma=d_1\sqrt{\frac{\mu}{\eta}}\ \ ,D_a=\frac{k_o}{d_1^2},F_r=\frac{c^2}{gd_1} \\ ,\ \frac{d_1^2\,\grave{p}(\grave{x})}{\lambda\mu c}=p\ ,B_r=P_r.E_c\ ,\ \ G_r=\frac{\rho\, g(\mathrm{T}_1-\mathrm{T}_0)\,\dot{\alpha}\,d_1}{\mu\, c},\ E_c=\frac{c^2}{(\mathrm{T}_1-\mathrm{T}_0)\,C_p}. \end{array}\right\} \qquad (12)$$

Where $\mathcal{H}$ is Hartmann number , R_e is Reynolds number, δ is Wave number , γ is Couple stress parameter , P_r is Prandtl number , D_a is Darcy number , F_r is Froude number, B_r is Brinkman number , E_c is Eckert number ,and G_r is Grashof number .

According to equations (1) and (2), the dimensionless shape of the peristaltic channel walls may be shown in $h_1^*(x)$ and $h_2^*(x)$

$$h_1^*(x) = 1 + kx + a\ \cos(2\pi x) \tag{13}$$

$$h_2^*(x) = -d - kx - b\ \cos(2\pi x + \phi_\circ) \tag{14}$$

Where $a = \frac{a_1^*}{d_1}$, $b = \frac{a_2^*}{d_1}$, $d = \frac{d_2}{d_1}$, $k = \left(\frac{\lambda \tan\tilde{\alpha}}{d_1}\right)$ is referred to as the channel's Non-uniform parameter and $\phi_\circ$ the relation $a^2 + b^2 + 2ab\cos\phi_\circ \leq (1+d)^2$

Where($\psi_\circ$) stream function of velocity components u^* and v^* that is dimensionless $u^* = \frac{\partial\psi_\circ}{\partial y}$ and $v^* = -\frac{\partial\psi_\circ}{\partial x}$, respectively, and satisfy the continuity equation (8).

In terms of stream function $\psi_\circ$, the dimensionless variables are specified in equations. (9), (10), and (11) were translated into the following equations.

$$R_e.\delta\left[\left(\frac{\partial\psi_\circ}{\partial y}.\frac{\partial}{\partial x} - \frac{\partial\psi_\circ}{\partial x}.\frac{\partial}{\partial y}\right)\frac{\partial\psi_\circ}{\partial y} + \frac{\partial^2\psi_\circ}{\partial x\partial y}\right] - \frac{\rho\grave{\Omega}^2 d_1^2}{\mu}\left(\frac{\partial\psi_\circ}{\partial y} + 1\right) + 2\grave{\Omega}R_e\delta^2\frac{\partial^2\psi_\circ}{\partial x\partial t^*} = -\frac{\partial p}{\partial x} + \delta^2\frac{\partial^3\psi_\circ}{\partial x^2\partial y} + \frac{\partial^3\psi_\circ}{\partial y^3} - \frac{1}{\gamma^2}\left(\delta^4\frac{\partial^5\psi_\circ}{\partial x^4\partial y} + 2\delta^2\frac{\partial^5\psi_\circ}{\partial x^2\partial y^3} + \frac{\partial^5\psi_\circ}{\partial y^5}\right) - \mathcal{H}^2\cos\Phi\left[\left(\frac{\partial\psi_\circ}{\partial y} + 1\right)\cos\Phi + \frac{\partial\psi_\circ}{\partial x}\ \delta\sin\Phi\right] - \frac{1}{D_a}\left(\frac{\partial\psi_\circ}{\partial y} + 1\right) + \frac{R_e}{F_r}\sin\tilde{\alpha} + G_r\ \theta\sin\tilde{\alpha} \tag{15}$$

$$R_e.\delta^3\left[\left(-\frac{\partial\psi_\circ}{\partial y}.\frac{\partial}{\partial x} + \frac{\partial\psi_\circ}{\partial x}.\frac{\partial}{\partial y}\right)\frac{\partial\psi_\circ}{\partial x} - \frac{\partial^2\psi_\circ}{\partial x^2}\right] + \frac{\rho\grave{\Omega}^2 d_1^2}{\mu}\delta^2\frac{\partial\psi_\circ}{\partial x} + 2\grave{\Omega}R_e\delta^2\frac{\partial^2\psi_\circ}{\partial y\partial t^*} = -\frac{\partial p}{\partial y} - \delta^2\left(\delta^2\frac{\partial^3\psi_\circ}{\partial x^3} + \frac{\partial^3\psi_\circ}{\partial y^2\partial x}\right) + \frac{\delta^2}{\gamma^2}\left(\delta^4\frac{\partial^5\psi_\circ}{\partial x^5} + 2\delta^2\frac{\partial^5\psi_\circ}{\partial x^3\partial y^2} + \frac{\partial^5\psi_\circ}{\partial y^4\partial x}\right) + \mathcal{H}^2\ \delta\ \sin\Phi\ \left[\left(\frac{\partial\psi_\circ}{\partial y} + 1\right)\cos\Phi + \frac{\partial\psi_\circ}{\partial x}\ \delta\sin\Phi\right] + \frac{\delta^2}{D_a}.\frac{\partial\psi_\circ}{\partial x} - \frac{R_e}{F_r}\ \delta\cos\tilde{\alpha} \tag{16}$$

$$R_e.\delta.P_r\left(\frac{\partial\psi_\circ}{\partial y}.\frac{\partial\theta_\circ}{\partial x} + \frac{\partial\theta_\circ}{\partial x} - \frac{\partial\psi_\circ}{\partial x}.\frac{\partial\theta_\circ}{\partial y}\right) = \left(\delta^2\frac{\partial^2\theta_\circ}{\partial x^2} + \frac{\partial^2\theta_\circ}{\partial y^2}\right) + B_r\left[4\delta^2\left(\frac{\partial^2\psi_\circ}{\partial x\partial y}\right)^2 + \left(\frac{\partial^2\psi_\circ}{\partial y^2} - \delta\frac{\partial^2\psi_\circ}{\partial x^2}\right)^2 + \frac{1}{\gamma^2}\left[\left(\delta^2\frac{\partial^3\psi_\circ}{\partial x^2\partial y} + \frac{\partial^3\psi_\circ}{\partial y^3}\right)^2 + \left(\delta^2\frac{\partial^3\psi_\circ}{\partial x^3} + \frac{\partial^3\psi_\circ}{\partial x\partial y^2}\right)^2\right]\right] + B_r\,\mathcal{H}^2\left[\left(\frac{\partial\psi_\circ}{\partial y} + 1\right)\cos\Phi + \frac{\partial\psi_\circ}{\partial x}\ \delta\sin\Phi\right]^2 \tag{17}$$

Cross differentiation from dimensionless equations is used to remove the pressure term. (17), (18), and (19) may be formulated in the context of stream function differential equation and temperature under low Reynolds approximations and long-wavelength assumptions($\delta << 1$) .

$$\frac{\partial^6\psi_\circ}{\partial y^6} - \gamma^2\frac{\partial^4\psi_\circ}{\partial y^4} + \gamma^2\frac{\partial^2\psi_\circ}{\partial y^2}\left[\mathcal{H}^2\cos^2\Phi + \frac{1}{D_a} - \frac{\rho\grave{\Omega}^2 d_1^2}{\mu}\right] = 0 \tag{18}$$

$$\frac{\partial^2\theta_\circ}{\partial y^2} + B_r\left[\left(\frac{\partial^2\psi_\circ}{\partial y^2}\right)^2 + \frac{1}{\gamma^2}\left(\frac{\partial^3\psi_\circ}{\partial y^3}\right)^2\right] + B_r\,\mathcal{H}^2\cos^2\Phi\left(\frac{\partial\psi_\circ}{\partial y}\right)^2 = 0 \tag{19}$$

The dimensionless boundary conditions in the wave frame are [5]:

$$\left.\begin{array}{l} \frac{\partial\psi_\circ}{\partial y}+\beta\frac{\partial^2\psi_\circ}{\partial y^2}=-1 \quad on\ y=h_1^* \\ \frac{\partial\psi_\circ}{\partial y}-\beta\frac{\partial^2\psi_\circ}{\partial y^2}=-1 \quad on\ y=h_2^* \\ \psi_\circ=\frac{F}{2}, \quad \theta_\circ=0 \ \ on\ \ y=h_1^* \\ \psi_\circ=-\frac{F}{2}, \quad \theta_\circ=1 \ \ on\ \ y=h_2^* \\ \frac{\partial^3\psi_\circ}{\partial y^3}=0\ on\ y=h_1^* and\ y=h_2^* \end{array}\right\} \qquad (20)$$

As a result of solving equations (18) and (19), the associated boundary conditions (20) are satisfied.

$$\psi_\circ=\frac{2e^{-ya_1}t_1}{a_3}+\frac{2e^{ya_1}t_2}{a_3}+\frac{2e^{-ya_2}t_3}{a_4}+\frac{2e^{ya_2}t_4}{a_4}+t_5+yt_6 \qquad (21)$$

$$\theta_\circ=r_1+yr_2+\frac{1}{2\gamma^2a_3^3a_4^3}\left(-\frac{1}{2a_1}e^{-2ya_1+3y(a_1+a_2)-y(a_1+3a_2)}(\mathcal{H}^2+2\mathcal{H}^2Cos[2\Phi]+\right.$$
$$\mathcal{H}^2Cos[4\Phi]+2i\mathcal{H}^2Sin[2\Phi]+i\mathcal{H}^2Sin[4\Phi]+4Cos[2\Phi]a_1^2+4iSin[2\Phi]a_1^2)\ldots \qquad (22)$$

It's possible to write the velocity as:

$$W=-\frac{2e^{-ya_1}a_1t_1}{a_3}+\frac{2e^{ya_1}a_1t_2}{a_3}-\frac{2e^{-ya_2}a_2t_3}{a_4}+\frac{2e^{ya_2}a_2t_4}{a_4}+t_6 \qquad (23)$$

The axial pressure gradient can be calculated once we've identified the stream function.

$$\frac{\partial p}{\partial x}=\frac{\partial^3\psi_\circ}{\partial y^3}-\frac{1}{\gamma^2}.\frac{\partial^5\psi_\circ}{\partial y^5}-\mathcal{H}^2\cos^2\Phi\left[\left(\frac{\partial\psi_\circ}{\partial y}+1\right)\right]-\frac{1}{D_a}\left(\frac{\partial\psi_\circ}{\partial y}+1\right)+\frac{R_e}{F_r}\sin\tilde{\alpha}+G_r\theta_\circ\sin\tilde{\alpha}+$$
$$\frac{\rho\grave{\Omega}^2d_1^2}{\mu}\left(\frac{\partial\psi_\circ}{\partial y}+1\right) \qquad (24)$$

$$\frac{\partial p}{\partial y}=0 \qquad (25)$$

In non-dimensional form, the pressure rise per wavelength Δp_* is defined as

$$\Delta p_*=\int_0^1\frac{\partial p}{\partial x}dx \qquad (26)$$

3.Volumetric flow rate

In the laboratory frame, the volumetric flow rate is equal to

$$\tilde{Q}=\int_{\widetilde{h_2}}^{\widetilde{h_1}}\tilde{U}\ (\tilde{X},\tilde{Y},\tilde{t})d\tilde{Y} \qquad (27)$$

where $\widetilde{h_1}$ and $\widetilde{h_2}$ are functions of $\tilde{X}$ and $\tilde{t}$.

In the wave frame, the volumetric flow rate is calculated:

$$q_\circ=\int_{\widetilde{h_2}}^{\widetilde{h_1}}\grave{u}(\grave{x},\grave{y})d\grave{y} \qquad (28)$$

The relationship between Q and q can is calculated as follows:

$$\tilde{Q}=q_\circ+c(\widetilde{h_1}-\widetilde{h_2}) \qquad (29)$$

The time-mean flow over a span of time T^* fixed in place $\bar{X}$ as

$$Q_\circ=\frac{1}{T^*}\int_0^{T^*}\tilde{Q}dt \qquad (30)$$

Using equation (29) in equation (30) the flow rate $Q_\circ$ has the From

$$Q_\circ=\frac{1}{T^*}\int_0^{T^*}q_\circ dt+c(\widetilde{h_1}-\widetilde{h_2})$$

$$= q_\circ + cd_1 + cd_2 + 2cx\lambda\ \tan\tilde{\alpha} + ca_1\ \cos(2\pi x) + ca_2\cos(2\pi x + \phi_\circ) \qquad (31)$$

The non-dimensional of equation (28) is provided by

$$\omega = F + 1 + d + 2kx + a\cos(2\pi x) + b\cos(2\pi x + \phi_\circ) \qquad (32)$$

where $\omega = \frac{Q_\circ}{\mathrm{cd}_1}$and F $= \frac{q_\circ}{\mathrm{cd}_1}$ has the expression in the form

$$F = \int_{h_2^*}^{h_1^*} \frac{\partial\psi_\circ}{\partial y}\mathrm{dy} = \psi_\circ(h_1^*) - \psi_\circ(h_2^*) \qquad (33)$$

4. Results and Discussion

This section focuses on " velocity"W, "temperature" $\theta_\circ$, " gradient of pressure " δP^*, "pressure rise" Δp_* , and "stream function" $\psi_\circ$. To get the numerical values corresponding to the above-mentioned analytical formulas, we utilized "MATHEMATICA " program.

4.1. The distribution of velocity

Now, we'll look at the effect of axial velocity (W) variation across the canal on several parameters. Note that the velocity is parabolic. In the center, the axial velocity rises with increasing rotation parameter " $\grave{\Omega}$", density "ρ", the width of the channel "d_1", Darcy number " D_a" and the magnetic field inclination angle "Φ", whereas the axial velocity reduces near the channel wall's edge, as seen in Figure 1 (a-e). According to Figure 1(f) "$\phi_\circ$", is shown to increase axial velocity in the middle of the canal while axial velocity lowers at one wall boundary and rises at the other. As can be seen in Figures 1(g-k), as " $\mathcal{H}$ ", "γ", "β", viscosity "μ", and " k" increase, the axial velocity decreases in the channel's middle while increasing near the channel's wall border.

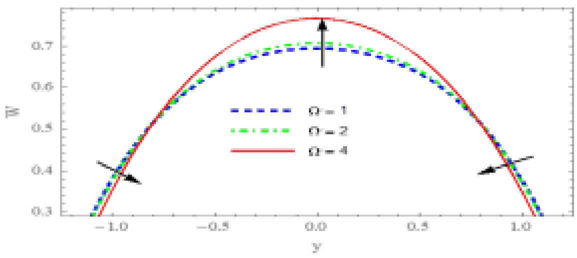

(a)

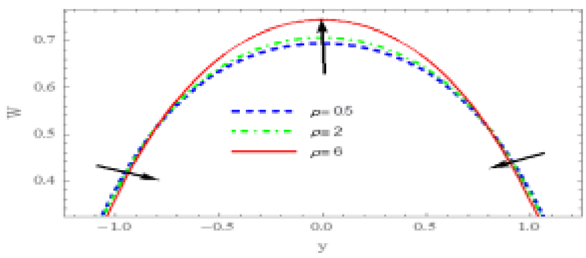

(b)

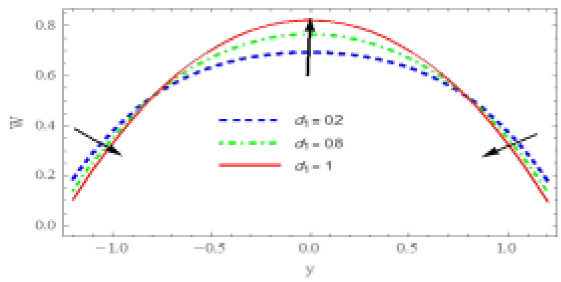

(c)

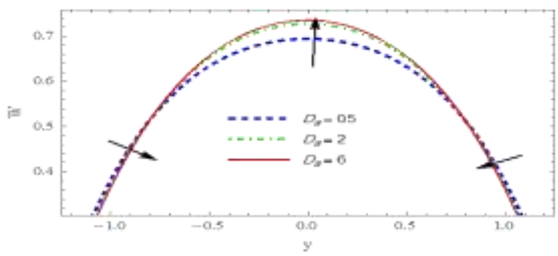

(d)

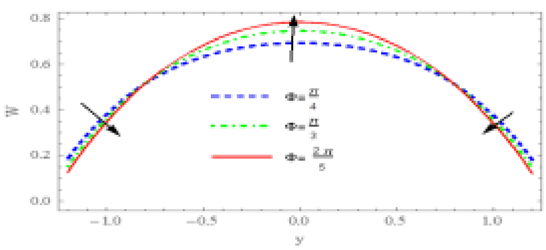

(e)

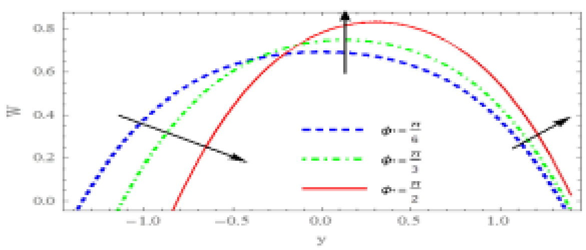

(f)

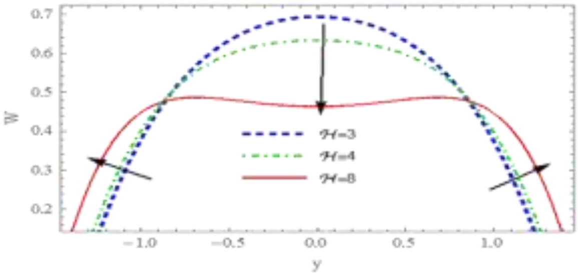

(g)

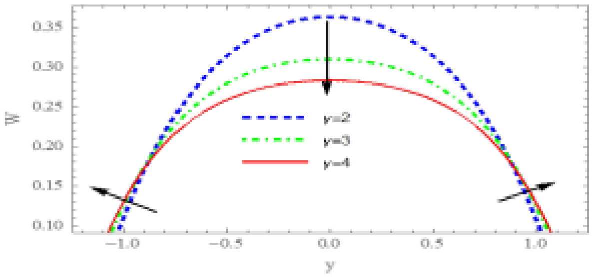

(h)

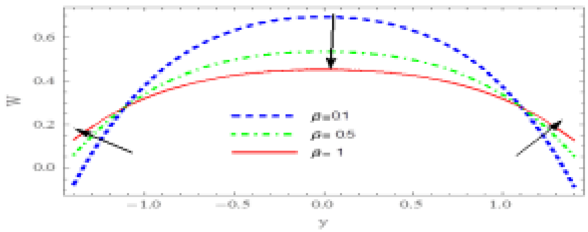

(i)

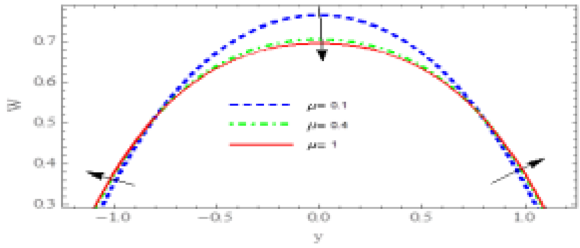

(j)

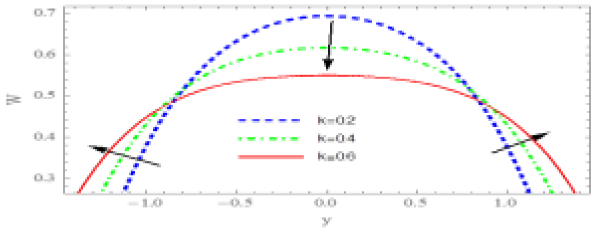

(k)

Figure 1. Variation the axial velocity "W" with different parameters $\{D_a = 0.5$, $\mathcal{H} = 3$, $\gamma = 2$, $a = 0.6$, $\mu = 0.1$, $\grave{\Omega} = 1$, $b = 0.7$, $\phi_\circ = \frac{\pi}{6}$, $d = 1$, $\beta = 0.1$, $\Phi = \frac{\pi}{4}$, $k = 0.2$, $x = 1$, $\rho = 0.5$, $F = 1$, $d_1 = 0.2\}$

4.2. Pumping characteristics

In this subsection, we will analyze the pressure through the channel.

4.2.1. pressure gradient" δP^* "

Each of the figures in this section illustrates the pressure gradient and the axial axis of fluctuation along the canal at one wavelength $x \in [0,1]$. Figures like this show that flow is restricted in the narrowing portion of channel $x \in [0.2,0.6]$. As a result, a larger pressure gradient is needed to achieve a normal flow. Because of the smaller pressure gradient in the larger area of the channel $x \in [0,0.2] \cup [0.6,1]$ fluid may pass readily. Figure 2(a-b) shows that when viscosity "μ" and the *H*artmann number "$\mathcal{H}$" raises, the pressure gradient also increases in size. This graphic shows that greater pressure is required to move some volume of fluid through the narrower region of the channel. When looking at channel parameters such as the magnetic field inclination angle "Φ" , the inclination"$\widetilde{\alpha}$" of the channel, rotation parameter "$\grave{\Omega}$" ,density "ρ" ,width of the channel "d_1" , Grashof numbers "G_r" ,*s*lip parameter"β", *D*arcy number "D_a" , *R*eynolds number"R_e",couple *s*tress "γ" , temperature "$\theta_\circ$", the phase difference "$\phi_\circ$" and Non-uniformity "k" as depicted in Figures 2(c –o), the pattern is the opposite. Because of the inclination, less pressure is needed to move liquids.

4.2.2. pressure rise" Δp_* "

Figures 3(a-o) show the relationship between pressure rise and volumetric flow rate. The connection between pressure rise and the rate of volumetric flow for each wavelength is seen to be linear. The whole region is considered into five parts (1) the peristaltic pumping region where($\Delta p_* > 0$, $F > 0$) (2) when ($\Delta p_* > 0$, $F < 0$), then it is a retrograde pumping region (3) augmented pumping (co-pumping) region where ($\Delta p_* < 0$, $F > 0$) (4) There is a co-pumping region where ($\Delta p_* < 0$, $F < 0$) (5) ($\Delta p_* = 0$)corresponds to the free pumping region.

Figure3 (a-b) shows the impact of viscosity "μ" and Hartmann number "$\mathcal{H}$ "on Δp_* on It has been noticed in the retrograde pumping region. The pumping rate increases as Hartmann number "$\mathcal{H}$"increases. Co-pumping reduces when in this region and increases in "$\mathcal{H}$ "and "μ" . Volumetric flow rate and pressure increase Δp_* are shown to be linearly related in Figures 3 (c - f) for a variety of Grashof numbers "G_r" , "R_e", " $\tilde{\alpha}$" and "$\theta_\circ$ ". We observed that a rise results in an increase in retrograde pumping rate and augmented pumping (co-pumping) region an increase in the pressure rise. Figures 3 (g - m) Graph shows that with an increase in rotation parameter " $\grave{\Omega}$" ,density "ρ" ,width of the channel "d_1", " D_a", "β", "γ" and" Φ " . the pumping rate decreases in the region of retrograde pumping while in the augmented pumping region found to increase. Figure 3 (n)shows an impact of channel non-uniform parameter "k"on Δp_*. It is observed that in a retrograde pumping region and a free pumping region ($\Delta p_* = 0$), the pumping rate decreases with an increase in "k". Figure 3 (o) depicts the effect of "$\phi_\circ$" on Δp_*. It is observed that in a retrograde pumping region and a free pumping region ($\Delta p_* = 0$), the pumping rate increases with an increase in"$\phi_\circ$" .

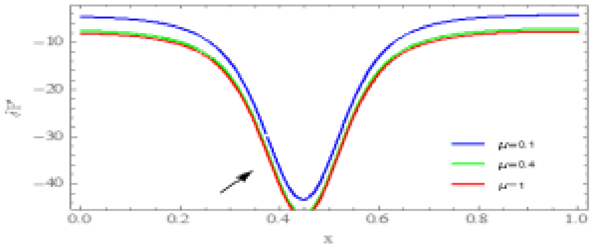

(a)

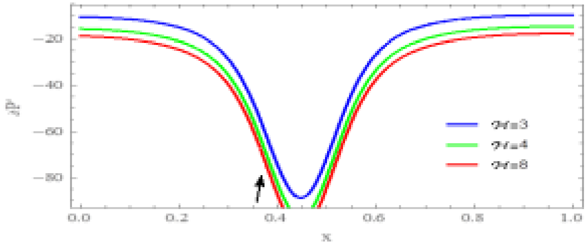

(b)

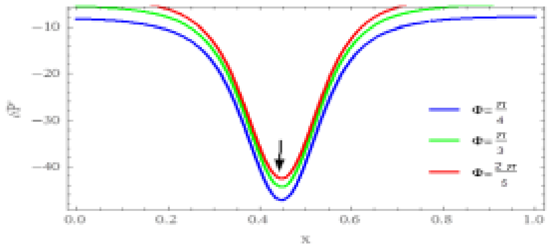

(c)

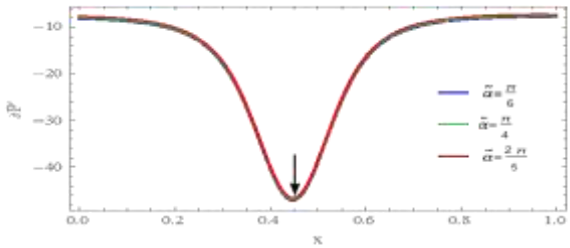

(d)

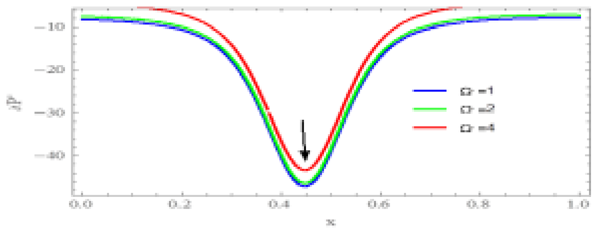

(e)

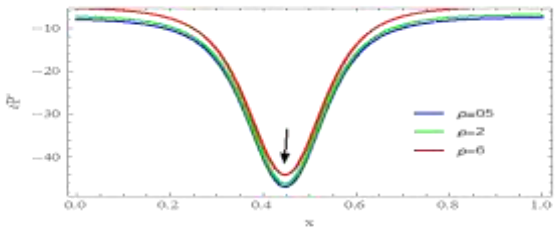

(f)

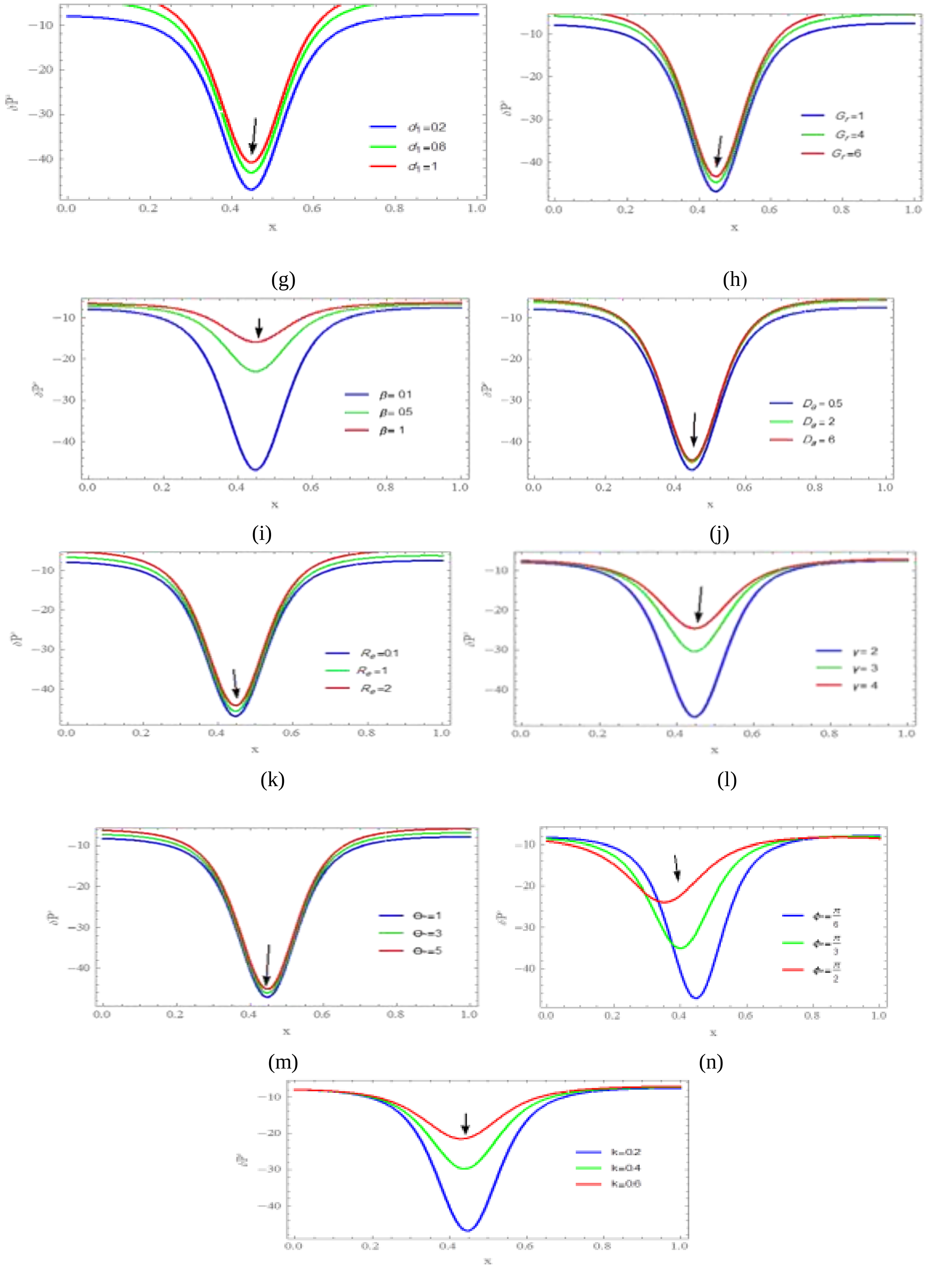

Figure 2. Variation the pressure gradient" δP^{*} with different parameters $\{D_a = 0.5, \mathcal{H} = 3, \gamma = 2, a = 0.6, \mu = 0.1, \grave{\Omega} = 1, b = 0.7, \phi_{\circ} = \frac{\pi}{6}, d = 1, \beta = 0.1, \Phi = \frac{\pi}{4}, k = 0.2, y = 1, \rho = 0.5, F = 0.1, d_1 = 0.2, F_r = 0.5, \tilde{\alpha} = \frac{\pi}{6}, G_r = 1, \Theta_{\circ} = 1\}$

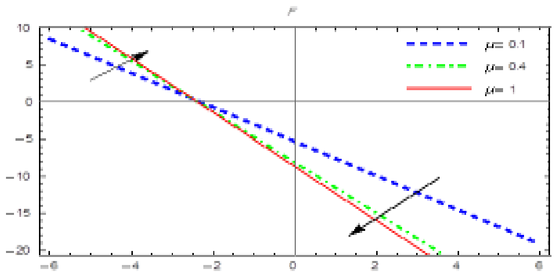

μ= 0.1
μ= 0.4
μ= 1

(a)

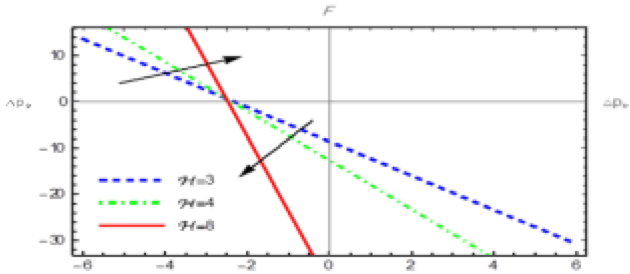

$\mathcal{H}$=3
$\mathcal{H}$=4
$\mathcal{H}$=8

(b)

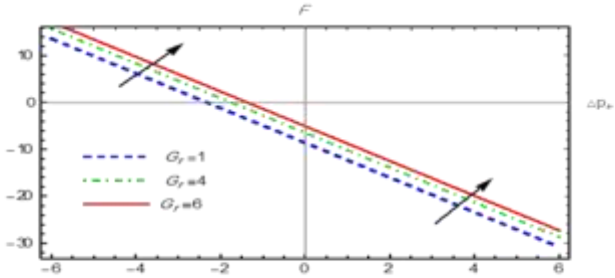

G_r=1
G_r=4
G_r=6

(c)

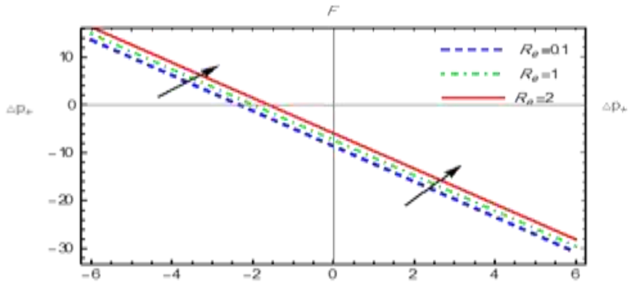

R_e=0.1
R_e=1
R_e=2

(d)

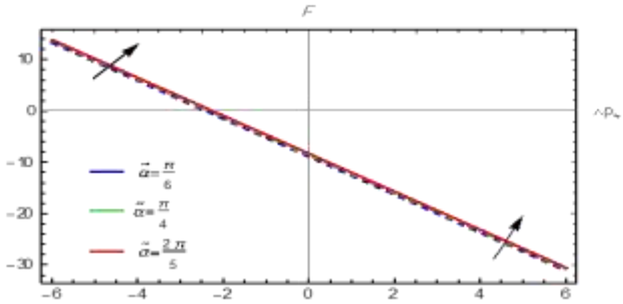

$\tilde{\alpha}=\frac{\pi}{6}$
$\tilde{\alpha}=\frac{\pi}{4}$
$\tilde{\alpha}=\frac{2\pi}{5}$

(e)

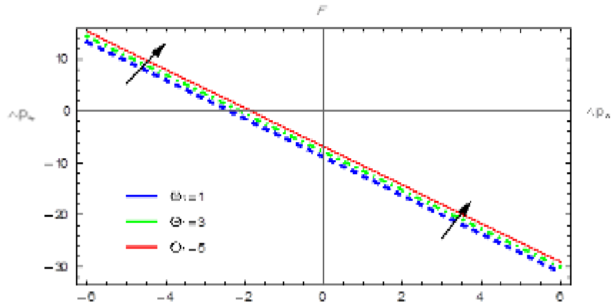

(f)

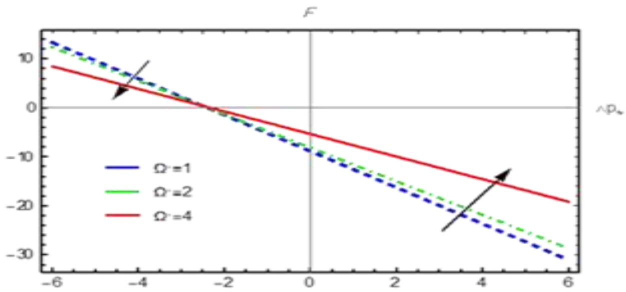

Ω=1
Ω=2
Ω=4

(g)

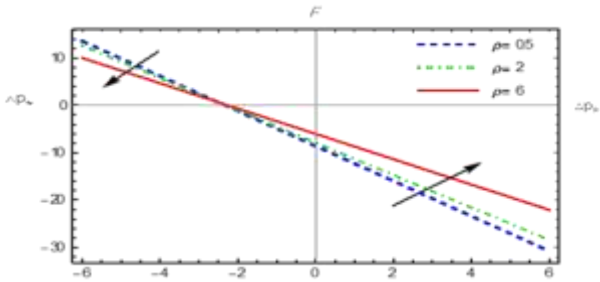

ρ= 05
ρ= 2
ρ= 6

(h)

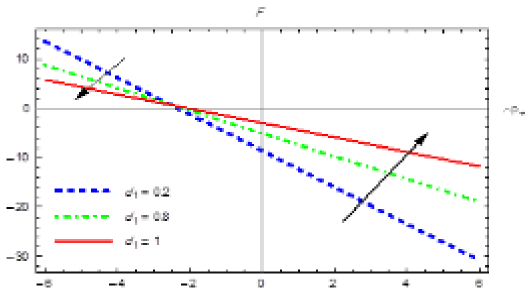

d_1 = 0.2
d_1 = 0.8
d_1 = 1

(i)

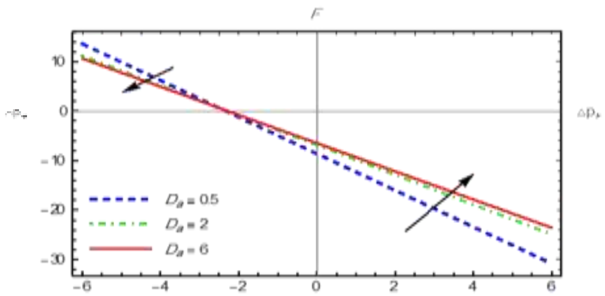

D_a = 0.5
D_a = 2
D_a = 6

(j)

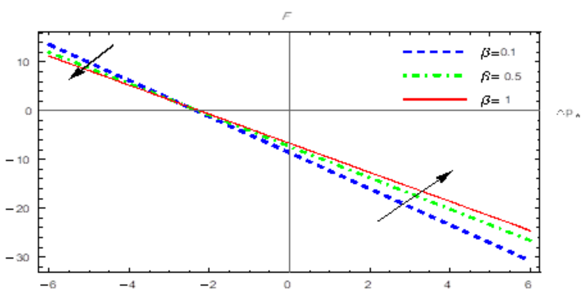

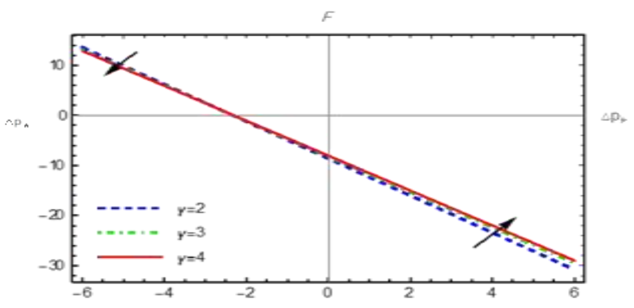

(k) (l)

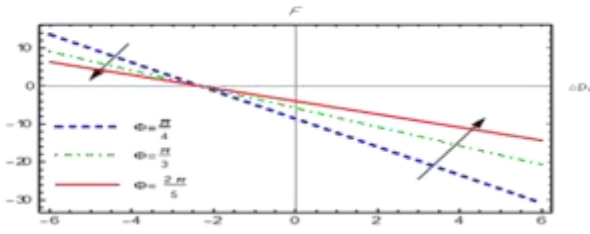

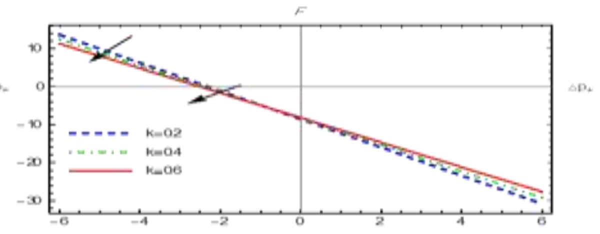

(m) (n)

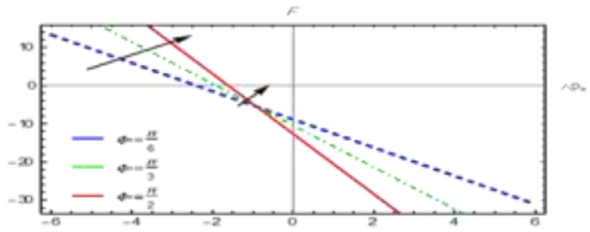

(o)

Figure 3 . Variation the pressure rise Δp_* with different parameters $\{D_a = 0.5\,, \mathcal{H} = 3\,, \gamma = 2\,, a = 0.6,\ \mu = 0.1\,, \grave{\Omega} = 1\,, b = 0.7\,, \phi_\circ = \frac{\pi}{6}\,, d = 1\,, \beta = 0.1\,, \Phi = \frac{\pi}{4}\,, k = 0.2\,, y = 1\,, \rho = 0.5\,, F = 0.1\,, d_1 = 0.2\,, F_r = 0.5\,, \tilde{\alpha} = \frac{\pi}{6}\,, G_r = 1\,, \Theta_\circ = 1\}$

4.3. temperature profile "$\theta_\circ$ "

An examination of the fluid temperature profile for a fixed value of x = 1 yields a parabolic temperature profile, with a higher graph in the middle. Fluids that have a high viscosity are more likely to convert kinetic energy into internal energy, which causes them to get hotter. There is no doubt about that. Its flow and movement resistance diminish with increasing temperature, a phenomenon caused by the tiny distances between molecules and the cohesive forces that exist between them. Figures 4 (a-g) show that the temperature increases values " $\grave{\Omega}$" , "ρ" , "d_1" " D_a" ,"H ", "k"and "B_r"increase, so does the temperature in the channel's center and temperature parabolic. The increase in temperature is accompanied by "B_r". $Brinkman$ number "B_r" of raised flow resistances given by shear. As parameter values "μ" , " "Φ " "β", "γ"and "$\phi_\circ$" increase, they show that the temperature decreases in Figures 4 (h-l).

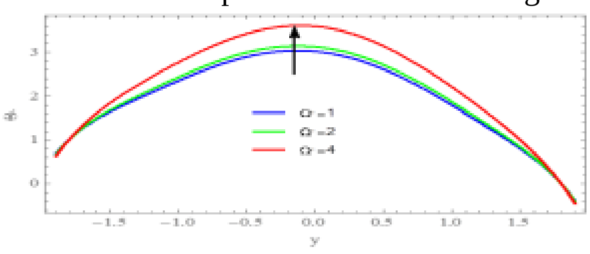

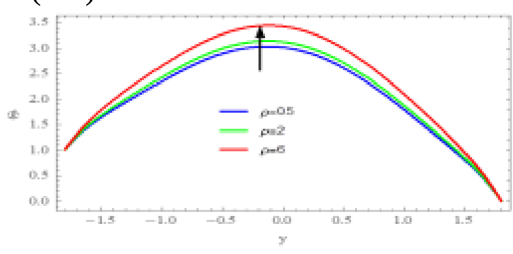

(a) (b)

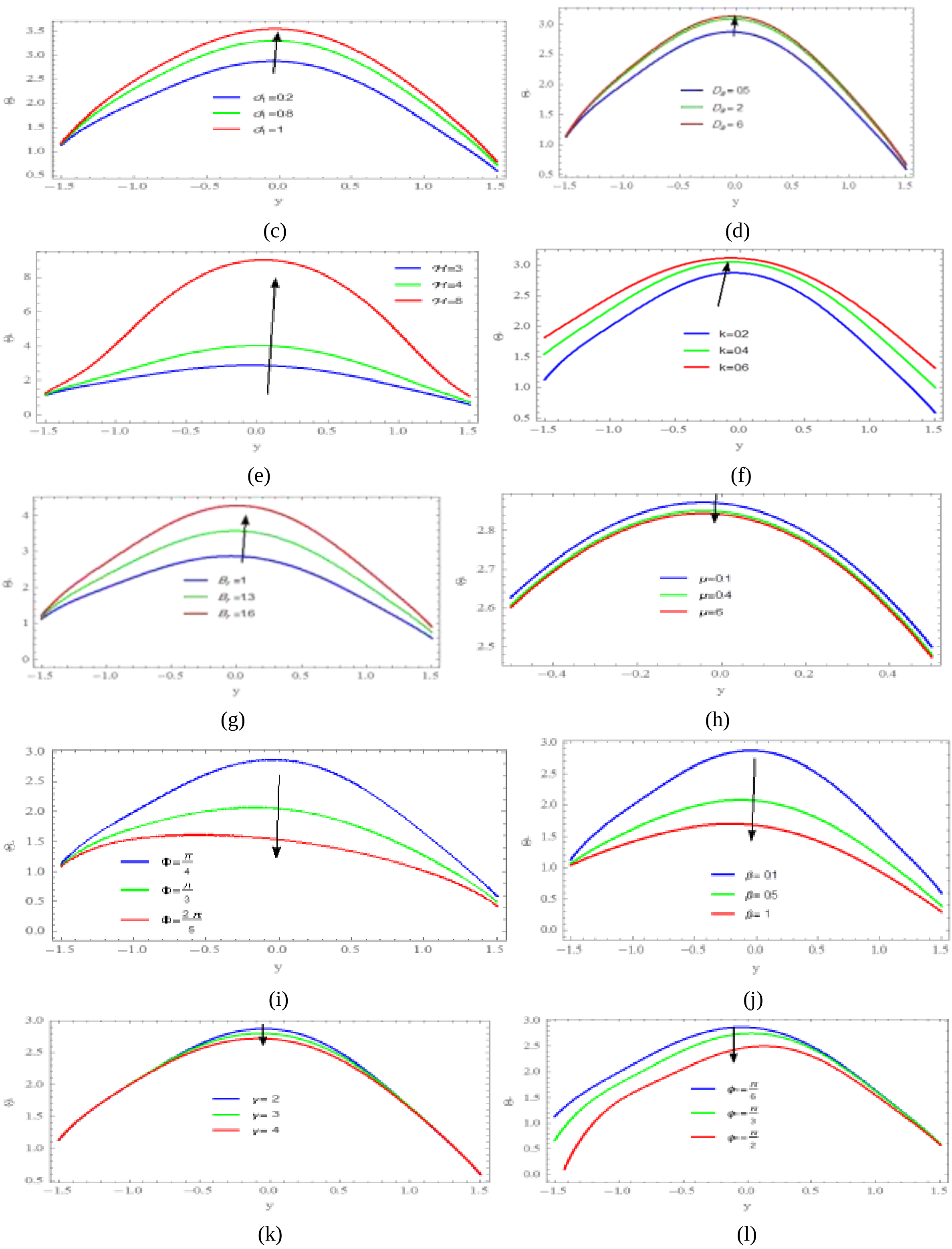

Figure 4. Variation the temperature "θ∘" with different parameters $\{D_a = 0.5, \mathcal{H} = 3, \gamma = 2, a = 0.6, \mu = 0.1, \grave{\Omega} = 1, b = 0.7, \phi_\circ = \frac{\pi}{6}, d = 1, \beta = 0.1, \Phi = \frac{\pi}{4}, k = 0.2, x = 1, \rho = 0.5, F = 0.1, d_1 = 0.2, B_r = 1\}$

4.4. The trapping phenomena

In order to explain the trapping phenomena, the formation of a circulating bolus of fluid, which is a closed streamline region, at the speed of the wave. There will be points in the wave frame where the fluid's velocity is zero due to the trapping phenomenon. The volumetric flow rate via a line linking any two places is computed by taking into account the difference in stream function values at the two sites in question, which is why studying streamline patterns is so important. Figures 5–15 indicate that bolus formation occurs from both sides of the center line in the extended region. Bigger and larger volumes of the trapped bolus can be extracted from the system by raising the strength of the magnetic field in Figures (5-9) (a, b, and c), as "Φ " , " $\grave{\Omega}$", "ρ" , "d_1" and " D_a". In Figures (10 and 11) (a ,b and c), as " $\phi_\circ$" and "μ" changes, so does the variation in streamlines.

According to our research, we've found that bolus sizes decrease"μ" and " $\phi_\circ$" increase. The Figure 12(a ,b and c) shows that the wall draws fluid in the widest section of the duct, but this fluid is pushed away from the wall in the narrower section and the bolus disappears in the central part as "β" increases. Graphing the non-uniformity parameter "k"of the asymmetric channel as shown in Figure 13(a, b, and c), when it is raised, the trapped bolus decreases in size and migrates downstream. These figures 14and15 (a, b, and c) demonstrate how In increasing the Hartman number "$\mathcal{H}$ ",and couple stress "γ" , the incidence of trapped bolus diminishes in size and vanishes in the direction of downstream, Another effect that may help protect red blood cells and other elements is the tendency to reduce bolus volume.

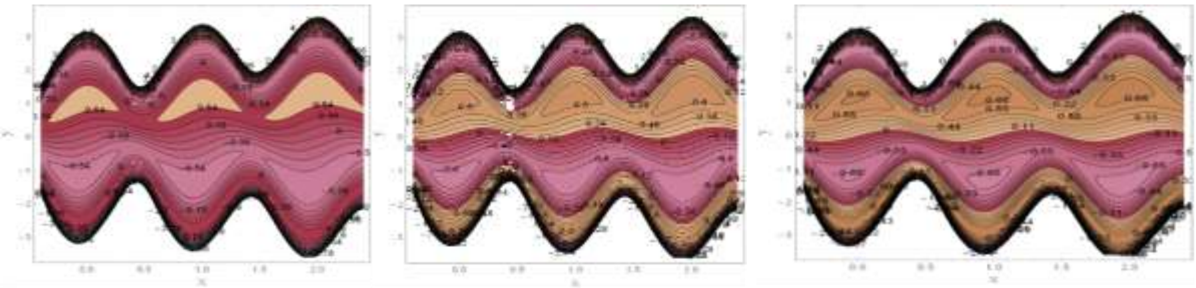

(a) (b) (c)

Figure 5. Distribution of streamlines " $\psi_\circ$" for (a) "Φ" = π/4 (b) "Φ" = π/3 (c) "Φ"= 2π/5

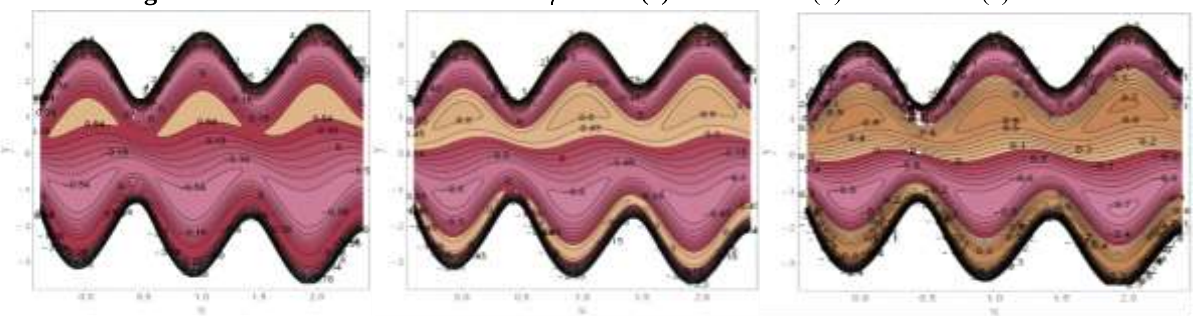

(a) (b) (c)

Figure 6. Distribution of streamlines " $\psi_\circ$" for (a) " $\grave{\Omega}$" =1 (b) " $\grave{\Omega}$" =2 (c) " $\grave{\Omega}$" =4

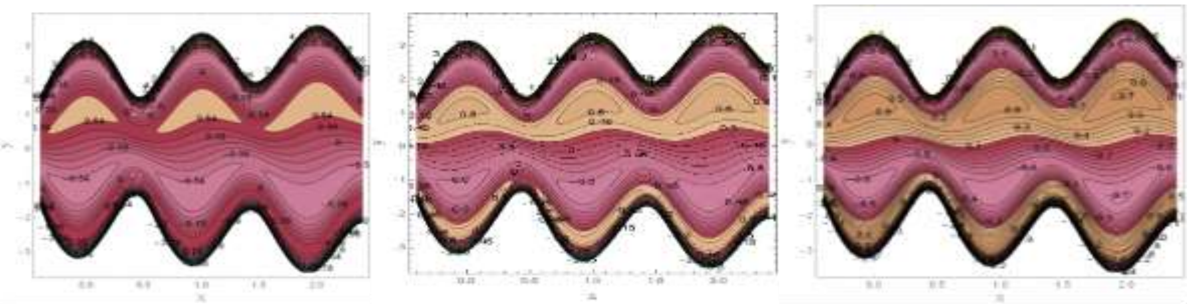

(a) (b) (c)

Figure 7. Distribution of streamlines " $\psi_\circ$" for (a) "ρ" = 0.5 (b) "ρ" = 2 (c) "ρ" = 6

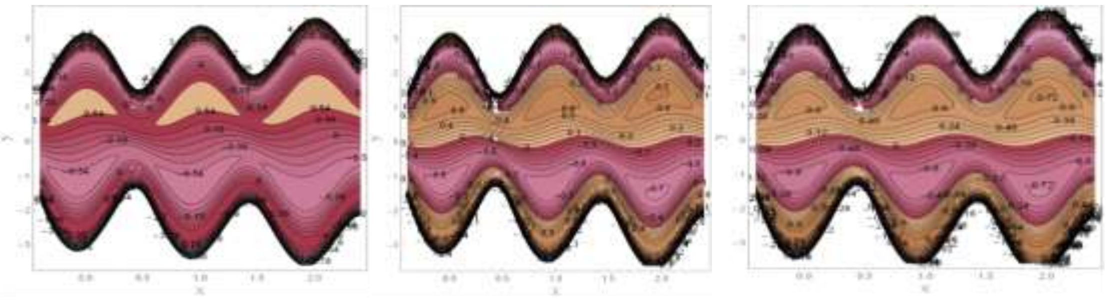

(a) (b) (c)

Figure 8. Distribution of streamlines " $\psi_\circ$" for (a) "d_1" =0.2 (b) "d_1" =0.8 (c) "d_1" =1

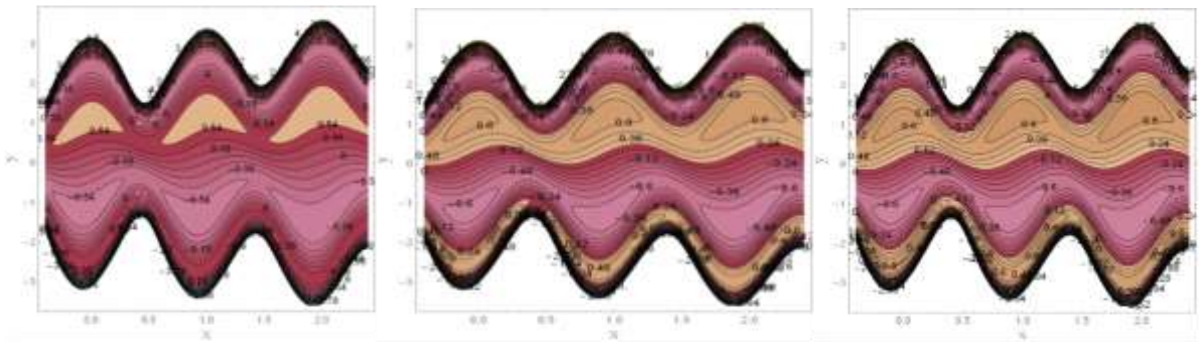

(a) (b) (c)

Figure 9 . Distribution of streamlines" $\psi_\circ$" for (a) " D_a" =0.5 (b) " D_a" =2 (c) " D_a" =6

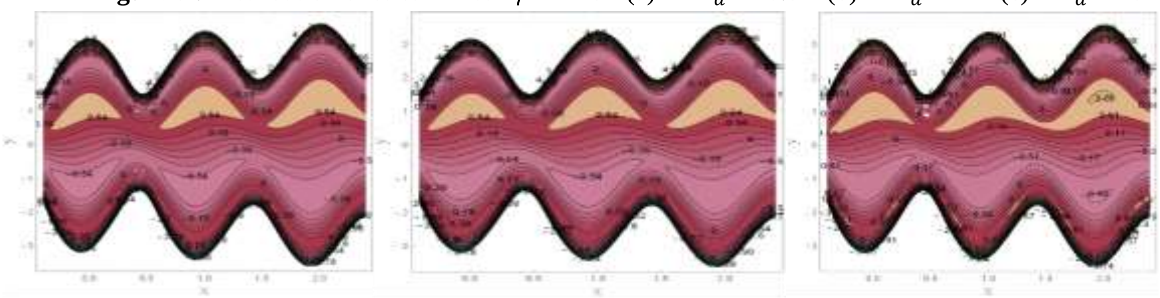

(a) (b) (c)

Figure 10 . Distribution of streamlines " $\psi_\circ$" for (a) "μ" =0.1 (b)"μ" =0.4 (c) "μ" =1

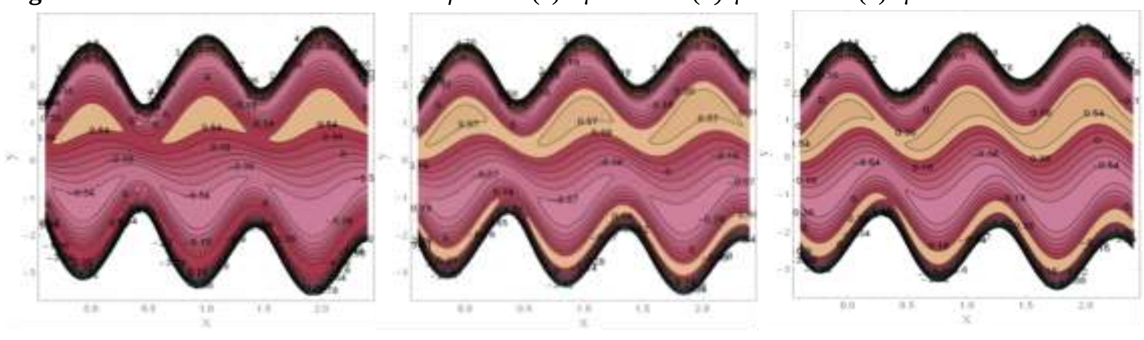

(a) **(b)** **(c)**

Figure 11. Distribution of streamlines " $\psi_\circ$" for (a) "$\phi_\circ$" $=\frac{\pi}{6}$ (b) "$\phi_\circ$" $=\frac{\pi}{3}$ (c) "$\phi_\circ$" $=\frac{\pi}{2}$

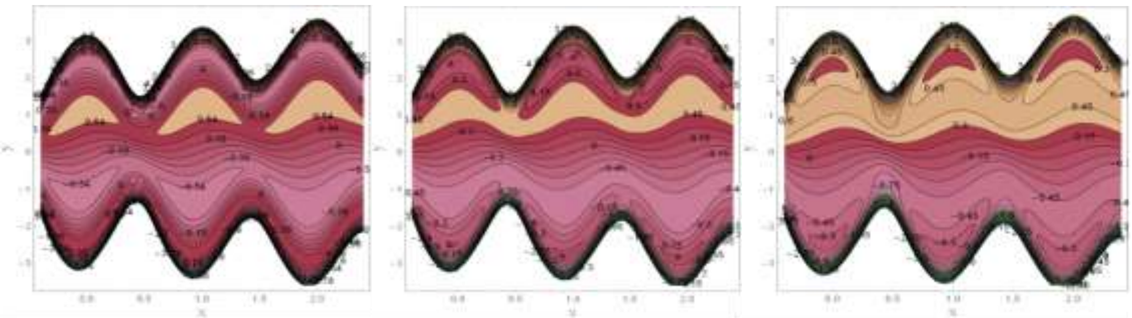

(a)

(b) (c)

Figure 12. Distribution of streamlines " $\psi_\circ$" for (a) "β" =0.1 (b) "β" =0.5 (c) "β" =1

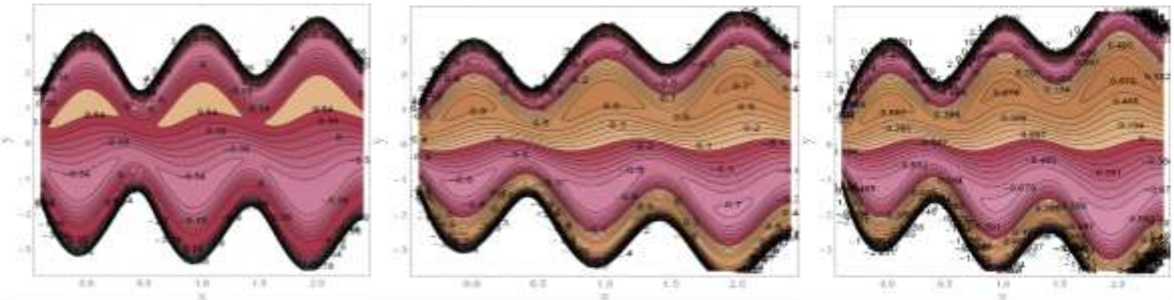

(a) (b) (c)

Figure 13. Distribution of streamlines " $\psi_\circ$" for (a) "k" =0.2 (b) "k" = 0.4 (c) "k"=0.6

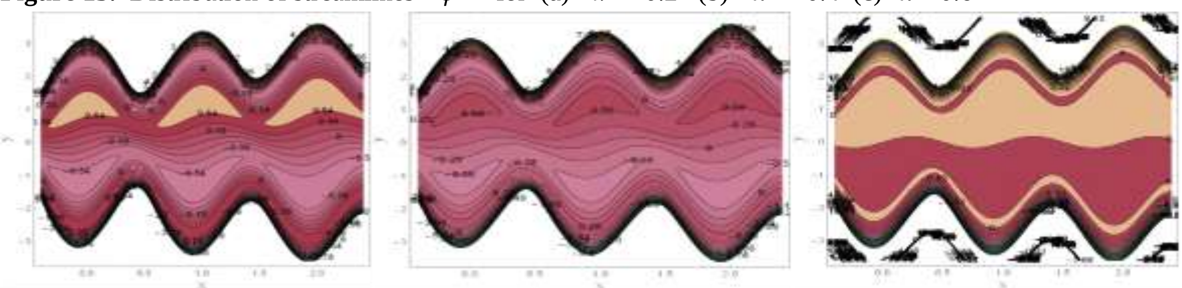

(a) (b) (c)

Figure 14. Distribution of streamlines " $\psi_\circ$" for (a) "$\mathcal{H}$ " =3 (b) "$\mathcal{H}$ " = 4 (c) "$\mathcal{H}$ "=8

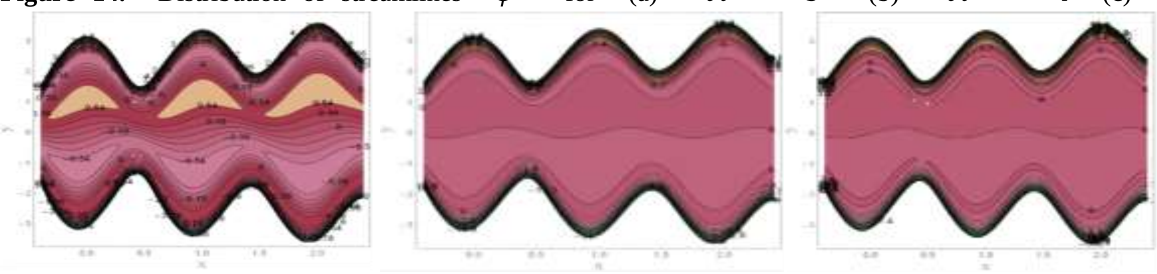

(a) (b) (c)

Figure 15. Distribution of streamlines " $\psi_\circ$" for (a) "γ" =2 (b) "γ" =3 (c) "γ" =4

5. Conclusions

In this research, we studied the effects of rotation and incline magnetohydrodynamics to investigate the effects of heat transfer and couple stress fluid as they move via an inclined asymmetric channel and porous medium under low Reynolds approximations and long-wavelength assumptions in the transport of bodily fluids by the use of non-Newtonian fluid models. Analytically, using Mathematica software. This investigation focused on studying the distribution of velocity, the pumping characteristics, the distribution of temperature, and the trapping phenomena.

1. It notes that the temperature and profile of velocity are parabolic.
2. There is a decrease in axial velocity "W" in the central region when increasing the viscosity "μ" , "γ" , "$\mathcal{H}$ ","β", and "k"", but there is a rise in velocity at the boundary of the channel wall.
3. There is an increase in axial velocity "W" in the central region when increasing the rotation parameter " $\grave{\Omega}$", "$\phi_\circ$" , density "ρ" , "Φ ", "d_1" and " D_a", but there is a decrease in velocity at the boundary of the channel wall.
4. When the viscosity "μ" , and Hartmann number "$\mathcal{H}$ "are increased, the pressure gradient " δP^* " increases, while " $\grave{\Omega}$", "Φ" , "β", "$\widetilde{\alpha}$", "G_r", " D_a", "γ", "$\phi_\circ$", "ρ", "k", "d_1" , "R_e" ,and "$\theta_\circ$ " decrease.
5. The connection between pressure rise " Δp_* "and volumetric flow rate for each wavelength is seen to be linear.
6. In retrograde pumping, increases " Δp_* " pressure rise with the increasing values the viscosity "μ" , "G_r","R_e" , "H ", "$\theta_\circ$ " ,"$\widetilde{\alpha}$" and "$\phi_\circ$", whereas it decreases with the rising values the rotation parameter " $\grave{\Omega}$", "Φ"," D_a" , "γ" , "β" ,density "ρ" , "d_1" ,and" k".
7. The temperature "$\theta_\circ$ " rises when the rotation parameter " $\grave{\Omega}$", density "ρ" , "d_1" , "k" , " D_a" , "$\mathcal{H}$ "and Brinkman number"B_r" all go up. It goes decrease when the inclination magnetic field angle "Φ", the slip parameter "β" , couple-stress parameter"γ" , phase difference "$\phi_\circ$" , and the viscosity "μ" all go up.
8. When the values of "$\mathcal{H}$ "and "γ" are increased, the trapped boluses are eliminated. The inclination magnetic field angle "Φ", " $\grave{\Omega}$", "ρ" , "d_1" and " D_a" have a increasing impact on the bolus size.

References

1. Mekheimer, Kh. S. Effect of induced magnetic field on peristaltic flow of a couple stress fluid. *Physics Letters A* **2008** , *372*, 4271-4278.

2. Kumar, P. magneto- rotatory Thermal Converction in Couple –stress Fluid. *Int.J.of Thermal and Fluid sciences* **2012**,*1*, 11-20.

3. Hassen, R. Y. ; Ali, H. A. Hall and Joule's heating Influences on Peristaltic Transport of Bingham plastic Fluid with Variable Viscosity in an Inclined Tapered Asymmetric Channel. *Ibn AL-Haitham Journal For Pure and Applied Sciences* **2021**, *34(1)* , 68-84.

4. Hummady, L. Z. ; Abbas, I. T. ; Mohammed, R. A. Inclined Magnetic Field of Non-uniform and Porous Medium Channel on Couple Stress Peristaltic Flow and application in medical treatment (Knee Arthritis). *Journal of Southwest Jiaotong University* **2019**, *54(4).*

5. Shit, G.C. ; Ranjit, N.K. Role of slip velocity on peristaltic transport of couple stress fluid through an asymmetric non-uniform channel: Application to digestive system. *Journal of Molecular Liquids* **2016,** *221*, 305-315.

6. Murad ,M.A. ; Abdulhadi, A.M. Influence of MHD on mixed convective heat and mass transfer analysis for the peristaltic transport of viscoplastic fluid with porous medium in tapered channel. *Journal of Al-Qadisiyah foe computer Science and Mathematics* **2020**,*12* ,79-90 .

7. Abdulla, Sh. A. ; Hummady, L. Z. Inclined magnetic field and heat transfer of asymmetric and Porous Medium Channel on hyperbolic tangent peristaltic flow. *Int. J. Nonlinear Anal. Appl.* **2021** ,*12*, 2359-2372 .

8. Ali, N.; Wang, Y.; Hayat T. ; oberlack , M. slip effects on the peristaltic flow of a third grade fluid in a circular cylindrical tube . *J. Appl. Mech* **2009** ,*76*, 011006-011015 .

9. Chaube, M.K.; Pandey, S.K. ; Tripathi, D. Slip effects on Peristaltic transport of a micropolar fluid . *Appl. Math. Sci* **2010** ,*4* ,2105-2117 .

10. Abdulhadi, A. M. ; Al-Hadad , A. H. Slip Effect on the Peristaltic Transport of MHD Fluid through a Porous Medium with Variable Viscosity. *Iraqi Journal of Science* **2015** ,*56*, 2346-2363.

11. Abdulhussain, H. ; Abdulhadi, A. M. Peristaltic Transport of Couple Stress Fluid through an Inclined Asymmetric and Non-Uniform Channel with Porous Medium. *International Journal of Science and Research (IJSR)* **2018** ,*7*,7-16.

12. Mohaisen, H. N. ; Abdalhadi, A. M. Effects of The Rotation and A Magnetic Field on The Mixed Convection Heat Transfer Analysis for The Peristaltic Transport of Viscoplastic Fluid Through A Porous Medium in Asymmetric Channel. *Journal of Physics: Conference Series* , 1963(1), 012165 , IOP Publishing **2021**.

13. Salih, A. W.; Habeeb, S. B.. Peristaltic Flow with Nanofluid under Effects of Heat Source, and Inclined Magnetic Field in the Tapered Asymmetric Channel through a Porous Medium. *Iraqi Journal of Science* **2022**, 4445-4459.

14. Abd-Alla, A .M. ; Abo-Dahab, S. M. Magnetic field and rotation effects on the peristaltic transport of a Jeffery fluid in an asymmetric channel. *Journal of Magnetism and Magnetic Materials* **2015** ,*374*, 680-689.

15. Abdulhadi, A. M .; Al-Hadad, A. H. Effects of rotation and MHD on the Nonlinear Peristaltic Flow of a Jeffery Fluid in an Asymmetric Channel through a Porous Medium . *Iraqi Journal of Science* **2016** ,*57,* 223-240.

16. Alshareef, T. Sh. Impress of rotation and an inclined MHD on waveform motion of the nonNewtonian fluid through porous canal. *Journal of Physics: Conference Series, 1591, IOP Publishing* **2020**.

17. Mohaisen, H. N. ; Abdulhadi, A.M. Effects of the Rotation on the Mixed Convection Heat Transfer Analysis for the Peristaltic Transport of Viscoplastic Fluid in Asymmetric Channel. *Iraqi Journal of Science* **2022**,*63* , 1240-1257.

18. Salih, A. W. ; Habeeb, S. B. Influence Of Rotation, Variable Viscosity And Temperature On Peristaltic Transport In An Asymmetric Channel. *Turkish Journal of Computer and Mathematics Education (TURCOMAT)* **2021**, *12(6),* 1047-1059.